

The commensurate magnetic excitations induced by band-splitting and Fermi surface topology in n-type Cuprates

H. Y. Zhang¹, Y. Zhou¹, C. D. Gong^{2,1}, and H. Q. Lin³

¹*National Laboratory of Solid State Microstructure,
Department of Physics, Nanjing University, Nanjing 210093, China*

²*Center for Statistical and Theoretical Condensed Matter Physics,
Zhejiang Normal University, Jinhua 321004, China*

³*Department of Physics and the Institute of Theoretical Physics,
Chinese University of Hong Kong, Hong Kong, China*

The antiferromagnetic correlation plays an important role in high- T_c superconductors. Considering this effect, the magnetic excitations in n-type cuprates near the optimal doping are studied within the spin density wave description. The magnetic excitations are commensurate in the low energy regime and further develop into spin wave-like dispersion at higher energy, well consistent with the inelastic neutron scattering measurements. We clearly demonstrate that the commensurability originates from the band splitting and Fermi surface topology. The commensurability is a normal state property, and has nothing to do with d-wave superconductivity. The distinct behaviors of magnetic excitation between the n-type and p-type cuprates are further discussed. Our results strongly suggest the essential role of antiferromagnetic correlations in the cuprates.

PACS numbers: 71.27.+a, 75.40.Gb 74.72.Ek, 75.30.Fv

I. INTRODUCTION

The parent compounds of the high- T_c -temperature superconductors are antiferromagnetic (AFM) Mott insulator. Superconductivity (SC) emerges when charge carriers (holes or electrons) are doped into the CuO_2 planes. As well known that the clear electron-hole asymmetry is found in the phase diagram. For hole doped case, the AFM and superconducting phases are separated by spin glass phase. In contrast, the AFM phase extends over a much wider range of doping and even coexists with SC in the electron doped cuprates¹. Due to proximity of antiferromagnetism and SC, it is generally believed that there exists intrinsic link between these two phases. The studies of the spin dynamics in n-type and p-type cuprates will shed light on the mechanism of superconductivity.

One of the most available techniques to study the spin dynamics is the inelastic neutron scattering (INS), which directly measures the magnetic excitations (MEs). Compared with the well studied p-type cuprate^{2,3}, the investigations on the MEs in n-type cuprates⁴⁻⁹ are much less due to the technical reason. A robust feature of MEs in n-type cuprates, i.e., the commensurate spin response, had been revealed by these INS measurements. The commensurability, characterized by the strongest intensity peaked at $\mathbf{Q} = (\pi, \pi)$, covers for a wide low-energy region near the optimal doped NCCO⁴ and PLCCO⁵. Further detecting shows that such commensurability in n-type cuprates exists for a wide doping range from the underdoping to heavy overdoping^{7,8}. More importantly, the commensurate MEs persist well above superconducting critical temperature T_c , indicating its non-superconducting origin. It gradually develops into the spin-wave-like dispersion centered around the \mathbf{Q} point at higher energy, analogous to its undoped parent compound⁵. In contrast, The well known 'hourglass'

type magnetic dispersion had been discovered in the p-type cuprates, where the commensurate peak can only be found at the resonance energy. Therefore, the two types of cuprates exhibit distinct spin response, indicating the intrinsic particle-hole asymmetry.

Theoretically, several works had been carried out to interpret the MEs features of n-type cuprates. Adopting the single band description with experimentally fitted parameters, Krüger *et al.* claimed that the fermiology random phase approximation (RPA) approach with a momentum independent (or weakly dependent) Coulomb repulsion cannot account the low-energy commensurability. Their numerical results indicated that the MEs in n-type case should be more incommensurate than that in p-type case¹⁰. Such conclusion may reveal the fact that the single band description is invalid in the n-type cuprates⁷. Ismer *et al.* showed that this may be improved by a strongly momentum dependent Coulomb repulsion with form of $U_q = U_0(\cos q_x + \cos q_y)$ ¹¹. However, such improvement is more likely originated from its sharply peaked form at (π, π) , which cannot be understood physically. Using a slave-boson mean-field approach, Li *et al.* showed that the commensurability can be established in the SC state¹². These above mentioned theoretical works are all based on the belief that the d-wave SC is response for the low energy commensurability. It is hard to image that the small superconducting gap can produce the wide energy range commensurability. The most important is that the commensurate phenomenon is also found in the normal state of n-type cuprates, where the d-wave SC disappears. The MEs had also been discussed within the frame work of coexisting of SC and AFM¹³. Commensurate ME had been subsequently obtained¹⁴. However, this result clearly contradicts with the stoner critition^{15,16}. Furthermore, recent INS data reveal a magnetic quantum critical point where the SC first ap-

pears, implying that the coexistence may not exist⁶. Additionally, as we mentioned above, the commensurability also exists in the state without long-range AFM order.

In this paper, we focus on the commensurate MEs in the n-type cuprates near the optimal doping. Its energy region is closely related to the strength of effective (π, π) -scattering. The commensurate peak disappears at magnetic resonance energy ω_{res}^M and develops into the spin-wave like dispersion. These features are qualitatively consistent with INS measurements. This commensurability is a normal state property, and has nothing to do with the superconductivity. We explicitly demonstrate that the commensurability is originated from the band splitting and Fermi surface topology. Therefore, the AFM correlation plays key roles in the n-type cuprates. The differences of MEs between the p-type and n-type cuprates are further discussed for comparison.

A spin-density wave (SDW) description is adopted to investigate the n-type cuprates near the optimal doping. Such description is first suggested by Armitage *et al.* based on the ARPES measurements on *NCCO*¹⁷. The underlying Fermi surface disappears around the hot-spot near the optimal doping, where the long-range antiferromagnetism is absent, strongly suggesting the existence of a $\mathbf{Q} = (\pi, \pi)$ -scattering. Parker *et al.* further proposed an effective energy band with $\xi_k^\eta = \epsilon'_k + \eta \sqrt{\epsilon_k^2 + V_{\pi, \pi}^2}$ ($\eta = 1$, and -1 for upper, and lower band, respectively)¹⁸, where $V_{\pi, \pi}$ is the strength of the effective \mathbf{Q} -scattering, representing the influence of the SDW. ϵ_k and ϵ'_k is the inter- and intra-lattice hopping term. This description well reproduces the $\sqrt{2} \times \sqrt{2}$ band folding and Fermi surface reconstruction^{19,20}, and its applications on the temperature evolution of optical conductivity²¹ and the Hall coefficient²² give qualitative agreement with experiments. Now, the model Hamiltonian is expressed as

$$H = \sum_{k\sigma} \epsilon'_k (d_{k\sigma}^\dagger d_{k\sigma} + e_{k\sigma}^\dagger e_{k\sigma}) + \sum_{k\sigma} \epsilon_k (d_{k\sigma}^\dagger e_{k\sigma} + hc.) - \sum_{k\sigma} \sigma V_{\pi, \pi} (d_{k\sigma}^\dagger d_{k\sigma} - e_{k\sigma}^\dagger e_{k\sigma}), \quad (1)$$

where, the two sublattices D and E with respective fermionic operator d and e are introduced due to SDW²³. $\epsilon_k = -2t(\cos k_x + \cos k_y)$, and $\epsilon'_k = -4t' \cos k_x \cos k_y - 2t''(\cos 2k_x + \cos 2k_y) - \mu$ with t , t' , and t'' are the fitting parameters for nearest-neighbor (NN), second-NN, and third-NN hopping. The summation is restricted in the AFM Brillouin zone. The quasiparticle dispersion ξ_k^η can be obtained by the rotation transformation, with corresponding weight factor $W^\eta = \frac{1}{2}(1 + \eta \sin 2\theta_k)$. Here, $\cos 2\theta_k = \frac{V_{\pi, \pi}}{\sqrt{\epsilon_k^2 + V_{\pi, \pi}^2}}$, and $\sin 2\theta_k = \frac{\epsilon_k}{\sqrt{\epsilon_k^2 + V_{\pi, \pi}^2}}$.

Here, we would like to emphasize that the long-range AFM order disappears near the optimal doping. As pointed by Motoyama *et al.* that the Neel temperature detected above $x = 0.134$ in *NCCO* originates from the region of samples that were not fully oxygen-annealed⁶. This means that the genuine long-range antiferromag-

netism does not coexist with superconductivity. However, the 2-dimensional AFM correlation remains. Unlike only several lattice-distant length in p-type cuprates²⁴, the AFM correlation is about tens lattice-distance in the optimal electron-doped cuprates⁶. In this sense, the AFM correlations in the n-type cuprates is similar to the long-range AFM order at least in the small scaling. Therefore, using a slowly fluctuating SDW order to describe the long-range AFM correlation is a considerable treatment. Though present SDW description is analogous to the form in the AFM phase¹³, the physics behind is essentially different.

The spin susceptibility under random phase approximation is

$$\chi_q(\omega) = \frac{\chi_q^0 - U(\chi_q^0 \chi_{q+Q}^0 - \chi_{q,q+Q}^0 \chi_{q+Q,q}^0)}{(1 - U\chi_q^0)(1 - U\chi_{q+Q}^0) - U^2 \chi_{q,q+Q}^0 \chi_{q+Q,q}^0}, \quad (2)$$

with U is a reduced Coulomb interaction due to the screening effect²⁵. The bare spin susceptibilities are

$$\begin{aligned} \chi_{q,q}^0 &= \sum_k \sin^2(\theta_{k+q} + \theta_k) (F_{--} + F_{++}) \\ &\quad + \sum_k \cos^2(\theta_{k+q} + \theta_k) (F_{-+} + F_{+-}) \\ \chi_{q,q+Q}^0 &= \sum_k (\cos 2\theta_k - \cos 2\theta_{kq}) (F_{--} - F_{++}) \\ &\quad - \sum_k (\cos 2\theta_k + \cos 2\theta_{kq}) (F_{-+} - F_{+-}) \end{aligned} \quad (3)$$

with $F_{\eta\eta'}$ is

$$F_{\eta\eta'} = \frac{1}{4} (f_{kq}^\eta - f_k^{\eta'}) \left(\frac{1}{\omega - \xi_{kq}^\eta + \xi_k^{\eta'}} \right), \quad (4)$$

where $f_k = 1/(1 + e^{\xi_k/kT})$ is the Fermi distribution function. In numerically, the doping level is fixed at $x = 0.15$, near the AFM quantum critical point⁶. $t = 250meV$, $t' = -50meV$, and $t'' = 20meV$ are adopted¹⁸. The best fitted effective \mathbf{Q} -scattering strength is $V_{\pi, \pi} = 100meV$, and it will be adjusted for necessary. The temperature is fixed at $T = 0.2meV$. We adopt a broaden factor Γ to calculate the spin susceptibility. The reduced Coulomb interaction is about $600meV \sim 760meV$, which is about $2 \sim 3t$. Our calculations are carried out on a mesh with 2048×2048 k-point in the full Brillouin zone.

The typical energy-evolution of the MEs $\Im \chi_q(\omega)$ is shown in Fig. 1. In the low-energy regime below $18meV$ (Fig. 1(a), (b)), the MEs are incommensurate with strong intensity at diagonal directions. Simultaneously, the intensity near \mathbf{Q} enhances gradually. In the intermediate-energy regime, the strongest intensity locates at the \mathbf{Q} point, leading to the so-called commensurability (Fig. 1(c), (d)). It maintains up to an critical energy about $88meV$ (Fig. 1(e)), where the strongest intensity $\Im \chi_q(\omega)$ in the normal state can be found, and is referred as the magnetic resonance ω_{res}^M . The total energy

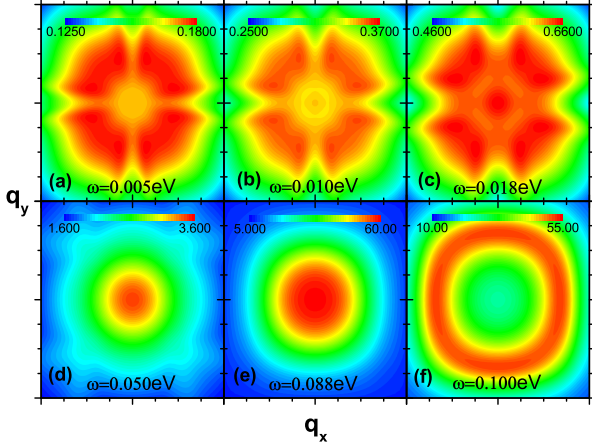


FIG. 1: The typical momentum distribution of MEs $\Im\chi_q(\omega)$ for different energy ω . Only the near \mathbf{Q} region are shown for clarification with $\frac{15\pi}{16} \leq q_x(q_y) \leq \frac{17\pi}{16}$. $U = 700\text{meV}$, the effective (\mathbf{Q})-scattering strength $V_{\pi,\pi} = 100\text{meV}$, and the broaden factor $\Gamma = 10\text{meV}$.

range for the commensurability is approximately 70meV for $\Gamma = 10\text{meV}$. This magnetic resonance is directly related to the fact that the real part in denominator of the RPA formula (Eq. 2) reduces to zero. Subsequently, it evolves into a ring-like incommensurability in the high-energy region with its radius expanding upon the further increased energy (Fig. 1(f)). For high enough energy, the MEs are incommensurate with strong intensity at the vertical directions (not shown).

Such features can be more clear in dispersion of the MEs at high symmetry scanning lines as shown in Fig. 2. A wide energy regime with commensurability exists for all selected U , manifesting its universal nature. The low-energy incommensurability increases slightly upon ω . Hence the commensurability cannot not be viewed as the overlap of two incommensurate peaks. It is an intrinsic feature of n-type cuprates. The low-energy incommensurability may be suppressed and even absent with enhanced U . For example, when $U = 0.76\text{V}$ (Fig. 2(c)), the MEs are still commensurate at low enough energy. Correspondingly, the magnetic resonance energy ω_{res}^M decreases down to 30meV for $\Gamma = 5\text{meV}$. The experimental discovered commensurability in $NCCO$ ⁴ and $PLCCO$ ^{7,8,26} near the optimal doping is more like similar to this case. The value of $U = 760\text{meV}$ is near the AFM stability, consisting with the fact that the optimal doping is near the AFM quantum critical point⁶.

The possible energy range of commensurability is mainly determined by the effective \mathbf{Q} -scattering potential $V_{\pi,\pi}$. For $V = 100\text{meV}$ and $\Gamma = 5\text{meV}$, it is about 48meV . This energy range decreases down to 10meV when the $V = 50\text{meV}$. However, the realistic energy range of commensurability may be substantially reduced for strong U due to the proximity of the AFM stability. It is only 30meV for stronger $U = 760\text{meV}$. For strong

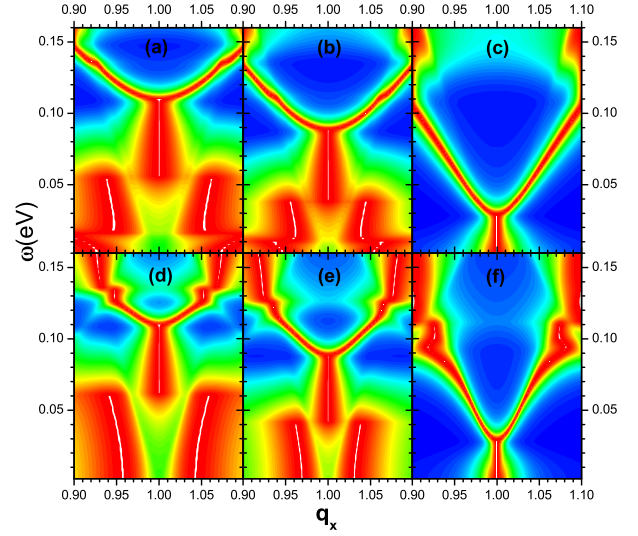


FIG. 2: The dispersion of the MEs $\Im\chi_q(\omega)$ along the high symmetry direction. Upper panels are for vertical direction with $q_y = \pi$, and lower panels are for the diagonal direction with $q_y = q_x$. From left to right is $U = 660\text{meV}$, 700meV , and 760meV , respectively. The effective \mathbf{Q} -scattering potential is $V_{\pi,\pi} = 100\text{meV}$ and the damping rate $\Gamma = 5\text{meV}$. All data had been renormalized by setting the strongest intensity at given ω as unit, denoted by the white lines.

enough $U \geq 770\text{meV}$ at given $V = 100\text{meV}$, the commensurability is entirely suppressed and only the ring-like magnetic feature remains. This situation is indeed an AFM state. Therefore, the ring-like feature at high-energy regime in the electron-doped cuprates shares the same origin as that in their parents compounds. In fact, those theories based on the long-range AFM order^{13,14} cannot account the commensurability found in $NCCO$ ⁴ and $PLCCO$ ⁷ due to Stone instability at $\omega = 0$ ¹⁶, unless some special control parameter is adopted. The energy range of commensurability also depends on the broaden factor Γ as comparing the data in Fig. 1 and Fig. 2 ((e) and (f)). However, this phenomenon is still present even a small $\Gamma = 1\text{meV}$ is adopted, which is less than the instrument resolution. Hence, the commensurability is an intrinsic and universal property of the electron-doped cuprates in the normal state.

The main difference in present work from the previous theoretical investigation by Krüger *et al.*¹⁰ is the influence of the AFM correlation is taken into account. The SDW description take the place of the single band description, producing a splitting two-band. Therefore, the commensurability is a directly result of the band-splitting. This can be also seem from the fact that commensurate energy region diminishes with the reduced $V_{\pi,\pi}$ as we shown before. As we known that the AFM correlation weakens with doping²⁷. In the heavy overdoping range, the AFM correlation disappears, i.e., $V_{\pi,\pi} = 0$, leading to the absence of band-splitting. Our results is then same as the work of Krüger *et al.*, the MEs become

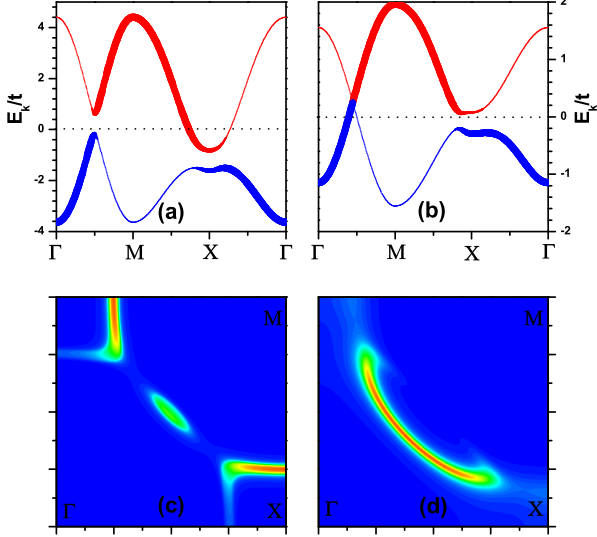


FIG. 3: The electron structure (upper panels) and Fermi surface (lower panels). (a), and (c) are for n-type cuprates with SDW description described in the text. (b), and (d) are for p-type cuprates with YRZ ansatz³⁰. The line thickness in (a), and (b) denotes the weight factor. The doping density is fixed at $x = 0.15$.

incommensurate, consisting with INS measurements⁷.

In the p-type cuprate, the MEs exhibit the well known 'hourglass' dispersion, the commensurate peak emerges at the single energy point ω_{res} . The underdoped p-type cuprates can also be described by the two-band description due to the opening of pseudogap²⁸, where the two bands near the antinodes are separated. Why do the two types of cuprates show significant particle-hole asymmetry? As well known that the Fermi surface is an 'arc' or hole pocket near the node point in the underdoped p-type cuprates²⁹, while it is an electron-pocket near antinodal point in the n-type cuprates even near the optimal doping as shown in Fig. 3. In fact, the two bands coincides at node point in p-type cuprates, which leads to the single-point commensurability at resonance energy. Furthermore, this can also interpret the commensurability exists in slightly overdoped n-type cuprates even the large-three-pieced Fermi surface¹⁷ forms because of the band splitting at nodes. Therefore, both the band splitting and Fermi surface topology play the important roles in the universal commensurability in the n-type cuprates.

As we stressed before, they both originate from the AFM correlation. Together with the previous theoretical works on the band structure^{19,20} and transport properties^{21,22}, we conclude that the AFM correlation plays essential roles in the cuprates.

The commensurate MEs remain in the presence of superconductivity. We introduce a phenomenological BCS-like pairing term $-\sum_k \Delta_k (d_{k\uparrow}e_{-k\downarrow} + e_{k\uparrow}d_{-k\downarrow} + h.c.)$ with standard *d*-wave symmetry $\Delta_k = \Delta(\cos k_x - \cos k_y)$. The resultant MEs change little, consistent with the INS observations. Therefore, the commensurability in n-type cuprate is a normal state property, and has nothing to do with SC. The commensurability had been also obtained in a single band description with *d*-wave superconductivity^{11,12}. Though the *d*-wave pairing produces two bands. However, the superconducting gap in the optimal doped n-type cuprates is only $3 \sim 4 meV$ ^{31,32}, too small to account for the wide energy range commensurability. It seems that the commensurability comes from the strong peaked factor U_q ¹¹ or J_q ¹² rather than the *d*-wave superconductivity in these theoretical investigations. More importantly, the commensurability is a normal state property, which can also be discovered well above the superconducting transition temperature T_c .

In conclusion, the magnetic excitations near the optimal doped n-type cuprates are studied within a spin-density wave description. The main features of magnetic excitations in the normal state are well established. Our analyses clearly demonstrate that the band splitting and the Fermi surface topology are the key for commensurability in n-type cuprates. This strongly suggests that the antiferromagnetic correlation plays important roles in cuprates. We emphasize that the commensurability is a normal state property, and has nothing to do with superconductivity. The qualitative agreement between the theoretical calculations and experimental data also suggests the validity of the spin-density wave description near the optimal doping where the long range antiferromagnetic order is absent. We also discuss the distinct behavior of magnetic excitations in the n- and p-type cuprates.

This work was supported by NSFC Projects No. 10804047, 11274276, and A Project Funded by the Priority Academic Program Development of Jiangsu Higher Education Institutions. CD Gong acknowledges 973 Projects No. 2011CB922101. HQ Lin acknowledges RGC Grant of HKSAR, Project No. HKUST3/CRF/09.

¹ N. P. Armitage, P. Fournier, and R. L. Greene, Rev. Mod. Phys. **82**, 2421 (2010).

² M. Fujita, H. Hiraka, M. Matsuda, M. Matsuura, J. M. Tranquada, S. Wakimoto, G. Xu, and K. Yamada, J. Phys. Soc. Jpn. **81**, 011007 (2012) (and reference therein).

³ J. Brinckmann and P. A. Lee, Phys. Rev. Lett. **82**, 2915 (1999); I. Eremin, D. K. Morr, A.V. Chubukov, K. H. Ben-

nemann, and M. R. Norman, Phys. Rev. Lett. **94**, 147001 (2005); G. Seibold and J. Lorenzana, Phys. Rev. B **73**, 144515 (2006); E. Demler and S.-C. Zhang, Phys. Rev. Lett. **75**, 4126 (1995).

⁴ K. Yamada, K. Kurahashi, T. Uefuji, M. Fujita, S. Park, S.-H. Lee, and Y. Endoh, Phys. Rev. Lett. **90**, 137004 (2003).

- ⁵ S. D. Wilson, P. Dai, S. Li, S. Chi, H. J. Kang, and J. W. Lynn, *Nature* (442), 59 (2006).
- ⁶ E. M. Motoyama, G. Yu, I. M. Vishik, O. P. Vajk, P. K. Mang, and M. Greven, *Nature* **445**, 186 (2007).
- ⁷ M. Fujita, M. Matsuda, S.-H. Lee, M. Nakagawa, and K. Yamada, *Phys. Rev. Lett.* **101**, 107003 (2008).
- ⁸ M. Fujita, M. Nakagawa, C. D. Frost, K. Yamada, *J. Phys. Conf. Ser.* **108**, 012006 (2008).
- ⁹ J. Zhao, F. C. Niestemski, S. Kunwar, S. Li, P. Steffens, A. Hiess, H. J. Kang, S. D. Wilson, Z. Wang, P. Dai, and V. Madhavan, *Nature Phys.* **7**, 719 (2011).
- ¹⁰ F. Krüger, S. D. Wilson, L. Shan, S. Li, Y. Huang, H.-H. Wen, S.-C. Zhang, P. Dai, and J. Zaanen, *Phys. Rev. B* **76**, 094506 (2007).
- ¹¹ J.-P. Ismer, I. Eremin, E. Rossi, and D. K. Morr, *Phys. Rev. Lett.* **99**, 047005 (2007).
- ¹² J. X. Li, J. Zhang, and J. Luo, *Phys. Rev. B* **68**, 224503 (2003).
- ¹³ Q. S. Yuan, T. K. Lee, and C. S. Ting, *Phys. Rev. B* **71**, 134522 (2005).
- ¹⁴ C. P. Chen, H. M. Jiang, and J. X. Li, *J. Phys. Condens. Matter* **22** 035701 (2010).
- ¹⁵ W. Rowe, J. Knolle, I. Eremin, P. J. Hirschfeld, *Phys. Rev. B* **86**, 134513 (2012).
- ¹⁶ J. R. Schrieffer, X. G. Wen, and S. C. Zhang, *Phys. Rev. B* **39**, 11663 (1988).
- ¹⁷ N. P. Armitage, D. H. Lu, C. Kim, A. Damascelli, K. M. Shen, F. Ronning, D. L. Feng, P. Bogdanov, and Z.-X. Shen, *Phys. Rev. Lett.* **87**, 147003 (2001).
- ¹⁸ S. R. Park, Y. S. Roh, Y. K. Yoon, C. S. Leem, J. H. Kim, B. J. Kim, H. Koh, H. Eisaki, N. P. Armitage, and C. Kim, *Phys. Rev. B*, **75**, 060501(R) (2007).
- ¹⁹ M. Ikeda, T. Yoshida, A. Fujimori, M. Kubota, K. Ono, Hena Das, T. Saha-Dasgupta, K. Unozawa, Y. Kaga, T. Sasagawa, and H. Takagi, *Phys. Rev. B*, **80**, 014510 (2009).
- ²⁰ H. Matsui, K. Terashima, T. Sato, T. Takahashi, S.-C. Wang, H.-B. Yang, H. Ding, T. Uefuji, and K. Yamada, *Phys. Rev. Lett.* **94**, 047005 (2005).
- ²¹ A. Zimmers, J. M. Tomczak, R. P. S. M. Lobo, N. Bonetemps, C. P. Hill, M. C. Barr, Y. Dagan, R. L. Greene, A. J. Millis, and C. C. Homes, *Europhys. Lett.* **70**, 225 (2005); A. Zimmers et al., *Phys. Rev. B* **76**, 064515 (2007).
- ²² Dagan, Y., M. M. Qazilbash, C. P. Hill, V. N. Kulkarni, and R. L. Greene, *Phys. Rev. Lett.* **92**, 167001 (2004).
- ²³ Any order with characteristic wave vector \mathbf{Q} would reproduce such band structure, but the SDW is most likely.
- ²⁴ M. A. Kastner, R. J. Birgeneau, G. Shirane, and Y. Endoh, *Rev. Mod. Phys.* **70**, 897 (1998).
- ²⁵ Y. Zhou, H. Q. Lin, and C. D. Gong, *Phys. Lett. A* **374**, 4065 (2010).
- ²⁶ M. Fujita, M. Matsuda, B. Fak, C. D. Frost, and K. Yamada, *J. Phys. Soc. Jpn.* **75**, 093704 (2006).
- ²⁷ Y. Zhou, H. Q. Lin, and C. D. Gong, *Phys. Rev. B* **77**, 092510 (2008).
- ²⁸ K.-Y. Yang, T. M. Rice, and F.-C. Zhang, *Phys. Rev. B* **73** 174501 (2006); Y. Zhou, H. Q. Lin, and C. D. Gong, *arXiv* **1011**, 3734v1.
- ²⁹ M. R. Norman, H. Ding, M. Randeria, J. C. Campuzano, T. Yokoya, T. Takeuchi, T. Takahashi, T. Mochiku, K. Kadowaki, P. Guptasarma, and D. G. Hinks, *Nature* **392**, 157 (1998); K. M. Shen, F. Ronning, D. H. Lu, F. Baumberger, N. J. C. Ingle, W. S. Lee, W. Meevasana, Y. Kohsaka, M. Azuma, M. Takano, H. Takagi, and Z.-X. Shen, *Science* **307**, 901 (2005).
- ³⁰ J. P. Carbotte, K. A. G. Fisher, J. P. F. LeBlanc, and E. J. Nicol, *Phys. Rev. B* **81**, 014522 (2010).
- ³¹ L. Shan, Y. L. Wang, Y. Huang, S. L. Li, J. Zhao, Pengcheng Dai, and H. H. Wen, *Phys. Rev. B* **78**, 014505 (2008).
- ³² Y. Dagan, M. M. Qazilbash, and R. L. Greene, *Phys. Rev. Lett.* **94**, 187003 (2005).